Electrochemically deposited transition metal dichalcogenide heterostructures as electrocatalysts

Manyepedza, Tshiamo; Auvray, Thomas; Friščić, Tomislav; Rees, Neil V.

DOI:
10.1016/j.elecom.2024.107678

Document Version
Publisher's PDF, also known as Version of record

Citation for published version (Harvard):
Manyepedza, T, Auvray, T, Friščić, T & Rees, NV 2024, 'Electrochemically deposited transition metal dichalcogenide heterostructures as electrocatalysts: Accelerated kinetics for the hydrogen evolution reaction', *Electrochemistry Communications*, vol. 160, 107678. https://doi.org/10.1016/j.elecom.2024.107678

Electrochemistry Communications 160 (2024) 107678

Contents lists available at ScienceDirect

Electrochemistry Communications

journal homepage: www.elsevier.com/locate/elecom

Electrochemically deposited transition metal dichalcogenide heterostructures as electrocatalysts: Accelerated kinetics for the hydrogen evolution reaction

Tshiamo Manyepedza [a], Thomas Auvray [b], Tomislav Friščić [b], Neil V. Rees [a,*]

[a] School of Chemical Engineering, University of Birmingham, Edgbaston, Birmingham B15 2TT, United Kingdom
[b] School of Chemistry, University of Birmingham, Edgbaston, Birmingham B15 2TT, United Kingdom

ARTICLE INFO

Keywords:
Transition metal dichalcogenides
Heterostructures
Hydrogen evolution
Reaction kinetics
Tafel analysis

ABSTRACT

Transition metal dichalcogenide (TMD) heterostructures have been discovered to have improved catalytic activity towards the hydrogen evolution reaction (HER). This study explores the stability and HER catalytic activity including reaction kinetics of heterolayers of different TMDs (MoS_2, $MoSe_2$ and WS_2). The stability of the heterolayers varied with those having an overlayer of electrodeposited MoS_2 being more stable as compared to those with $MoSe_2$ overlayer which degraded with each scan in acidic media. Investigation into the HER kinetics of the heterolayers involved Tafel analysis and electrochemical rate constant calculation. There was an improvement in Tafel values calculated in comparison to reported values for these heterolayers. WS_2/MoS_2 and $MoSe_2/MoS_2$ heterolayers registered rate constants of $(3.20 \pm 0.10) \times 10^{-4}$ cm s^{-1} and $(1.73 \pm 0.03) \times 10^{-4}$ cm s^{-1} respectively, which was an improvement of up to an order of magnitude compared to the reported rate constant of electrodeposited MoS_2 of $(3.17 \pm 0.30) \times 10^{-5}$ cm s^{-1}. All this highlights the improved HER catalytic activity of the heterolayers.

1. Introduction

Transition metal dichalcogenides (TMDs) play a major role in chemical sensing, energy storage, semiconductors and capacitors and have lately gained attention in both electro and photocatalysis [1–3], due to their effective catalysis of the hydrogen evolution reaction (HER) as well as their low cost in comparison to platinum group electrocatalysts [4–7]. Their two-dimensional (2D) structure makes it possible to alter their physical and chemical properties through means such as doping, nanostructuring and exfoliation which [7–9], in terms of electrocatalysis, results in increased active edge sites that improve the catalytic activity for the hydrogen evolution reaction.

Various TMDs have been investigated as possible HER electrocatalysts: molybdenum disulfide (MoS_2) has been shown to be promising due to its stability and high catalytic activity for HER [10–14], as well as molybdenum diselenide ($MoSe_2$), a narrow bandgap, semiconductor with low Gibbs energy that makes it suitable for HER [15–18]. Like most 2D TMDs, these materials have an inactive basal plane which limits their catalytic activity hence the need to alter and modify their structures to increase the active (edge) sites for HER catalysis [19–21]. As an alternative to increasing edge sites, engineering a phase transition from the 2H → 1 T metallic phase has found some success in improving the HER performance [22–26].

Recently, studies investigated TMD heterolayered structures: that is, having two layers of stacked TMDs to modify the bandgap of the resulting heterolayer to improve photoelectrocatalysis towards HER [27–30]. Computational methods were used to investigate and predict how stacking one TMD on top of the other could influence the bandgap both positively and negatively depending on whether the valence band maximum and conduction band minimum were located in the different layers [29,30]. Hydrothermal and chemical vapor deposition methods have been used in constructing heterostructures and these have been shown to display improved electrocatalytic hydrogen evolution behaviour [31,32]. Some TMD heterolayers can also be fabricated from electrodeposited TMD films, for example the heterolayers resulting from electrodeposited films of MoS_2 and $MoSe_2$ have displayed an enhanced proton reduction activity [33]. Another benefit is the cost-effective deposition process compared to energy intensive methods such as chemical vapor deposition for creating the TMD films/layers [19,33,34]. Electrochemical deposition makes use of affordable and readily

* Corresponding author.
E-mail address: n.rees@bham.ac.uk (N.V. Rees).

https://doi.org/10.1016/j.elecom.2024.107678
Received 8 January 2024; Received in revised form 2 February 2024; Accepted 6 February 2024
Available online 9 February 2024

obtainable precursors along with standard electrochemical techniques to efficiently make the TMD layers on a substrate support such as glassy carbon, indium tin oxide (ITO) or fluorine doped tin oxide (FTO) [35].

In this study, we investigate the HER performance of different TMD heterolayers resulting from both nanoparticulate and electrodeposited forms. A base particle layer of one type of TMD was dropcast onto an ITO/glassy carbon substrate and the second TMD layer was then electrochemically deposited on top to create the heterolayer. For the electrodeposited form, a base layer of one type of TMD is electrodeposited onto glassy carbon substrate, after which an overlayer of a different TMD is electrodeposited on top of it. The catalytic effect of the resulting TMD heterolayer on the HER was tested through linear sweep voltammetry along with their stability in acidic media. From the voltammograms, Tafel and reaction kinetics analysis was conducted to gain insight into the HER kinetics as well as to compare the catalytic activity of the different heterolayers. SEM-EDS and XPS were used to characterise the heterostructures and to confirm the chemical composition of the TMDs used.

2. Experimental

The following chemicals were purchased commercially and used without further purification: ammonium tetrathiomolybdate (>99 %), molybdenum (IV) sulfide nanoparticles (90 nm, 99 % trace metal basis), ammonium tetrathiotungstate (>99 % trace metal basis), tungsten (IV) sulfide nanoparticles (90 nm, 99 % trace metal basis), potassium sulfate (99.0 %), sodium perchlorate (>98 %, all from Sigma Aldrich), potassium chloride (99.0–100 %, Alfa Aesar), sodium hydroxide (97 %, Alfa Aesar), sodium selenite (>99 %, Fisher Chemical), molybdic acid (>85 %, Honeywell), sulfuric acid (95–98 %, Acros Organics) and molybdenum (IV) selenide (powder form, Ossila Ltd). All solutions were made using ultrapure water with a resistivity of not less than 18.2 MΩ cm (MilliQ, Millipore), and were thoroughly degassed with nitrogen (oxygen-free, BOC Gases plc) before each experiment and a nitrogen atmosphere maintained throughout the experiments.

All voltammetric experiments were carried out using a standard three-electrode cell comprising of a saturated Ag/AgCl reference (IJ Cambria Ltd), a graphite rod (Goodfellow Cambridge Ltd) counter, and glassy carbon (3 mm and 5 mm diameters, BASi Inc) working electrode. The working electrode was thoroughly polished sequentially with alumina slurries of decreasing size from 3 μm to 0.5 μm on microcloth lapping pads (Buehler Inc, USA). Cyclic voltammetry was performed using an Autolab PGSTAT302N potentiostat running Nova 2.1 software and analysis conducted through Excel and OriginPro 2022.

Electrochemical deposition of the molybdenum disulfide (MoS_2), molybdenum diselenide ($MoSe_2$) and tungsten disulfide (WS_2) films was performed in an oxygen free electrochemical cell via cyclic voltammetry. For the electrodeposition of MoS_2, the cell consisted of a saturated Ag/AgCl reference, graphite rod counter electrode and a glassy carbon working electrode and the solution contained 2 mM $(NH_4)_2MoS_4$ and 0.1 M $NaClO_4$ [10,11,36]. The same cell set-up was used for the electrodeposition of WS_2 but with a 10 mM $(NH_4)_2WS_4$ and 0.1 M KCl solution [19]. For $MoSe_2$ electrodeposition, a saturated calomel (SCE) reference was used and indium tin oxide (ITO) glass as the working electrode in a solution containing 0.05 M H_2MoO_4, 0.01 M Na_2SeO_3, 0.1 M $NaClO_4$ and adjusted to pH 6.5 with NaOH [33]. The nanoparticle layers were formed through dropcasting a 5 μL aliquot of the nanoparticle suspension on the electrode surface and leaving it to dry under a light source. $MoSe_2$ was purchased in powder form (<3mm particles) and then crushed to submicron sizes before being made into a suspension for dropcasting. The powder (150 mg) was reduced in size by grinding it in a 15 mL stainless steel jar from Form-Tech Scientific with two 7 mm stainless steel balls at 2500 rpm for 5 min using a FlackTek SpeedMixer™ (model DAC 330-100 Pro) and a custom-made jar holder. Analysis of each sample powder through XPS confirmed that no contamination due to the steel was detectable. Dynamic light scattering (DLS) was conducted using a Zetasizer Advanced Series-Ultra (Malvern Panalytical) to get the particle size distribution of the $MoSe_2$ powder.

Characterization of the heterolayer materials was conducted by a scanning electron microscope with energy dispersive spectroscopy (SEM-EDS) using a Hitachi TM3030 tabletop electron microscope. X-Ray photoelectron spectroscopy was performed using a Kratos Liquid Phase Photoelectron Spectroscopy (LiPPS) with a mono-chromated AI Kα X-ray source (1486.6 eV) operated at 10 mA emission current and 12 kV anode potential (120 W). Wide resolution scans were run with a step size of 0.5 eV and pass energy of 160 eV and high-resolution scans were run with a step size of 0.1 eV and a pass energy of 20 eV. High resolution scans were carried out for the photoelectron peaks from the detected elements in the wide spectra, and the data was analysed using CASA XPS software (version 2.3.23). Spectroscopic ellipsometry was used to determine the heterolayer thickness, conducted at three different angles (65°, 70° and 75°) using an alpha-SE (J.A Woollam Co. Inc) ellipsometer and the resulting data analysed and modelled using CompleteEASE software (J. A Woollam Co. Inc).

3. Results and discussion

3.1. Heterolayer formation and stability

Heterolayer samples were fabricated from combinations of two different transition metal dichalcogenides (TMDs) to explore their HER catalytic activities compared to the individual layers of the starting TMDs. Two methods of forming the heterolayers were used: first, where the heterolayer consisted of a dropcast nanoparticle layer with an electrodeposited layer of a different TMD on top ('NP/L'), and second where the heterolayer was formed was by sequential electrodeposition of layers of the two different TMDs ('L/L'). Since the particulate and electrodeposited forms of the TMDs have different morphologies (crystalline vs amorphous), these two methods produced samples with potentially different interactions at the NP-L or L-L interface.

The first heterolayer fabricated was the $MoSe_2/MoS_2$ (NP/L) consisting of MoS_2 film electrodeposited on top of a layer of $MoSe_2$ particles on a glassy carbon (GC) electrode surface. An aliquot of 5 μL of a suspension of molybdenum diselenide powder in deionised water (concentration of 3.9 mM) was drop cast onto a 3 mm GC electrode and left to dry under light source. The mechanochemically milled $MoSe_2$ particles had an average size of 240 nm with the size distribution ranging from 68 nm to 330 nm. The dropcast $MoSe_2$ particles had approximately 76 % area coverage of the GC surface, calculated from the suspension concentration and volume dropcast. The modified electrode was then placed in a solution of 2 mM $(NH_4)_2MoS_4$ and 0.1 M $NaClO_4$ and cycled at a voltage scan rate of 50 mV s^{-1} for 50 cycles between 0.4 V and −1.1 V (vs Ag/AgCl) to electrodeposit a film of MoS_2 onto the $MoSe_2$ NP layer. Fig. 1 shows the resulting voltammogram with the expected oxidative and reductive peaks at −0.3 V and −0.8 V (vs Ag/AgCl) respectively as a result of the redox processes below [10,11,34]:

$$[MoS_4]^{2-} \rightarrow MoS_3 + 1/8S_8 + 2e^- \quad (1)$$

$$[MoS_4]^{2-} + 2H_2O + 2e^- \rightarrow MoS_2 + 2HS^- + 2OH^- \quad (2)$$

The MoS_2 deposition voltammogram on $MoSe_2$ layer was identical to the voltammogram of MoS_2 deposition on bare GC (Figure S3). A further study onto the MoS_2 deposition cycles was conducted (in supporting information) to investigate the effects of deposition cycles/ film thickness on HER scans as well as determining the optimum number of cycles for full coverage of the electrode surface. It was found that 50 CV cycles for the electrochemical deposition were sufficient for full coverage and forming a stable heterolayer.

The $MoSe_2/MoS_2$ (NP/L) modified electrode was then tested for hydrogen evolution reaction (HER) catalytic activity and stability in acid solution through a series of cyclic voltammograms (CV). To

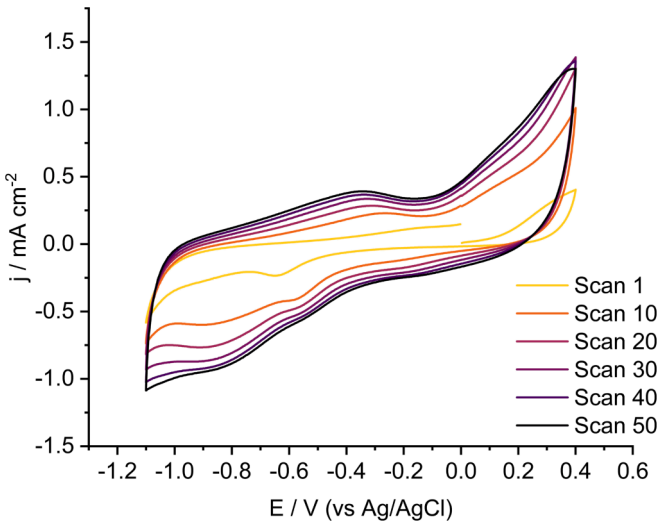

Fig. 1. Cyclic voltammogram of the electrodeposition of MoS_2 onto $MoSe_2$ modified glassy carbon electrode in a solution of 2 mM $(NH_4)_2MoS_4$ and 0.1 M $NaClO_4$ at a scan rate of 50 mV s^{-1}.

determine the stability of the heterolayer, 10 successive CV scans were conducted in a solution of 10 mM H_2SO_4 and 0.1 M K_2SO_4 to observe any changes in the scan and onset potential for HER. Fig. 2(A) shows that the onset potential remained approximately constant for the 10 scans and no obvious degradation of the heterolayer was observed thus confirming that the previously reported high stability of electrodeposited MoS_2 in acidic conditions is not affected by the presence of the underlying dropcast $MoSe_2$ NPs [11,37,38]. These studies highlighted how stable an electrodeposited layer of MoS_2 is through repeated cycling in various conditions without observing any noticeable changes in overpotential during the scans. The electrochemical deposition of MoS_2 in this study was conducted in a similar manner to these studies [11,37], hence the similar high stability observed in sulfuric acid solution during HER scans. Another study was carried out to determine the stability of dropcast $MoSe_2$ particles during the hydrogen evolution reaction. The dropcast $MoSe_2$ particles were observed to be unstable in the acid solution when conducting HER voltammetry (details given in the Supporting Information), where degradation of the layer was noticed as early as the second CV scan. The $MoSe_2$ layer dissolved into the solution with each scan until only the bare glassy carbon surface remained. This is not the case for the $MoSe_2/MoS_2$ (NP/L) heterolayer thanks to the stable overlayer of MoS_2 film which insulates the $MoSe_2$ layer thereby ensuring that the heterolayer remains intact during HER scans.

The other TMD heterolayers investigated were $MoS_2/MoSe_2$ (NP/L), WS_2/MoS_2 (NP/L), $WS_2/MoSe_2$ (NP/L) and $MoS_2/MoSe_2$ (L/L). The stability of these heterolayers were also investigated in pH 2 solution for HER and the results are shown on Fig. 2 ($WS_2/MoSe_2$ is given in supporting information). Those with an overlayer of $MoSe_2$ (B & D) have low stability compared to those with MoS_2 overlayers. The degradation of the heterolayer from the glassy carbon surface for both $MoS_2/MoSe_2$ and $WS_2/MoSe_2$ occurred after the first scan and continued with each run/scan. This degradation can be seen in Fig. 2 as the onset potential progressively moves to higher overpotentials with each cycle, tending towards the response for a bare GC surface. Electrodeposited $MoSe_2$ films have been observed to be less stable in acidic media for HER (Fig. S2) and adding that to a dropcasted layer of WS_2 and MoS_2 had no

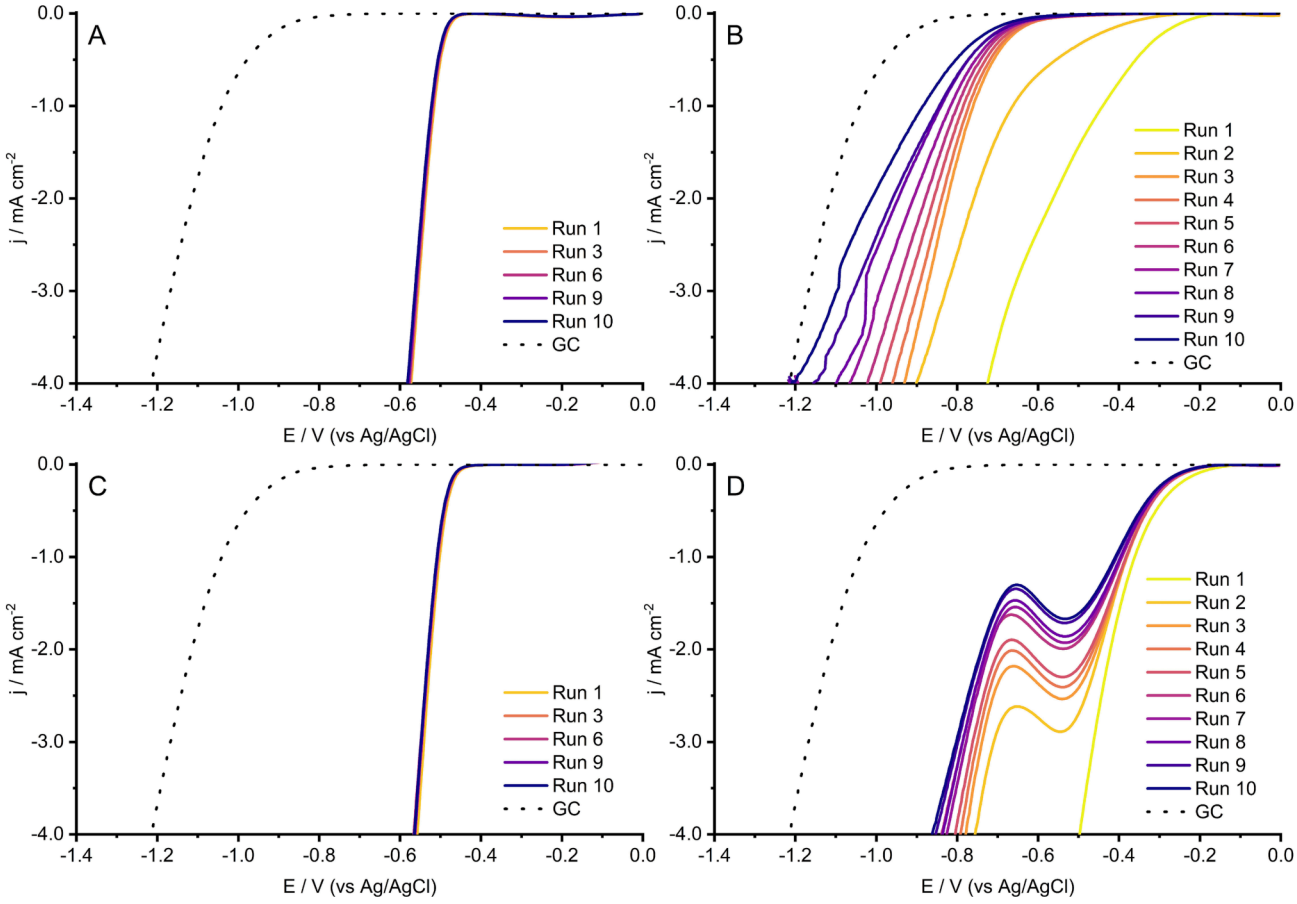

Fig. 2. Stability of the different heterolayers in 10 mM H_2SO_4 and 0.1 M K_2SO_4 (A) $MoSe_2/MoS_2$(NP/L), (B) $MoS_2/MoSe_2$(NP/L), (C) WS_2/MoS_2(NP/L), (D) $MoS_2/MoSe_2$(L/L). Each heterolayer was subjected to 10 successive scans at a voltage scan rate of 20 mV s^{-1}.

positive effect on the stability of the resulting heterolayer.

3.2. HER activity

After determining the stability of the different heterolayers, their catalytic effects towards the HER were evaluated. The heterolayers were created with the aim of increasing active sites for adsorption of hydrogen as well improving charge transportation due to the heterostructure [32,38,39]. Heterostructure formation has been reported to result in increased active edge sites and channels for charge transportation thus enhancing the electrical conductivity of the heterolayer, which all positively affects electrocatalytic activity [31,40,41]. The additional active edge sites are due to the increased surface area of the heterolayer as well as formation of defects at the heterointerfaces [42]. Catalytic activities of the two forms (particle-dropcast and electrodeposited forms) of TMDs making up the heterolayer were compared with that of the heterolayer, using linear sweep voltammetry (LSV) at a voltage scan rate of 20 mV s^{-1} in a solution of 10 mM H_2SO_4 and 0.1 M K_2SO_4 (see Fig. 3). Of the four combinations studied, $MoSe_2/MoS_2$ (NP/L) and WS_2/MoS_2 (NP/L) displayed a response indicative of improved kinetics over the electrodeposited layer (MoS_2) alone. MoS_2 has been the TMD of choice for most HER studies with its excellent catalytic activity and the ability to be modified to improve catalytic activity [6,9]. Of the many different structural forms of MoS_2, the electrodeposited form can be easily modified to change the number of trilayers formed by adjusting the cyclic voltammetry conditions. This combined with the formation of MoS_2 heterolayers results in improved HER activity thus showing the benefits of forming heterolayers.

A similar heterolayer response was reported in previous studies looking into TMD heterostructures which revealed increased electrocatalytic ability for HER [31,32,38]. One study investigated $MoSe_2/MoS_2$ heterostructure fabricated from thin sheets of the TMDs and this heterostructure showed a lowered overpotential needed to generate 10 mA cm^{-2} as compared to the component layers as well as improved electrocatalytic activity [38]. For $MoS_2/MoSe_2$ (NP/L), $WS_2/MoSe_2$ (NP/L) and $MoS_2/MoSe_2$ (L/L) (Supporting Information, Fig. S6), the current response was shifted to higher overpotentials (i.e., slower kinetics) compared to the electrodeposited layer ($MoSe_2$) alone. Electrodeposited $MoSe_2$ displays an earlier onset for HER than electrodeposited MoS_2 but is less stable in acid solutions (see above).

It was observed that the dropcast layers did not influence the stability of the electrodeposited overlayer, as degradation of the $MoS_2/MoSe_2$ and $WS_2/MoSe_2$ samples followed that of $MoSe_2$, with rapid increase of overpotential on consecutive CVs and reverting to a response akin to bare GC after less than 10 scans. Similarly, the samples with MoS_2 overlayers had similar stability to MoS_2 itself, albeit less catalytic than $MoSe_2$. A visual comparison of the heterolayers is shown on Fig. 4, having an overlay of the HER scans using the different heterolayers.

Tafel analysis was conducted for the heterolayers used and the resulting Tafel slopes along with onset potentials were determined. The reaction mechanism for HER is assumed to involve a series of steps which may be restricted by either the Volmer, Heyrovsky or Tafel steps as the rate determining steps and their associated Tafel slope values are as follows (Table 1) [19,43–45]:

Table 2 highlights the calculated Tafel slope values for HER due to the heterolayers. These provide an indication of the rate determining

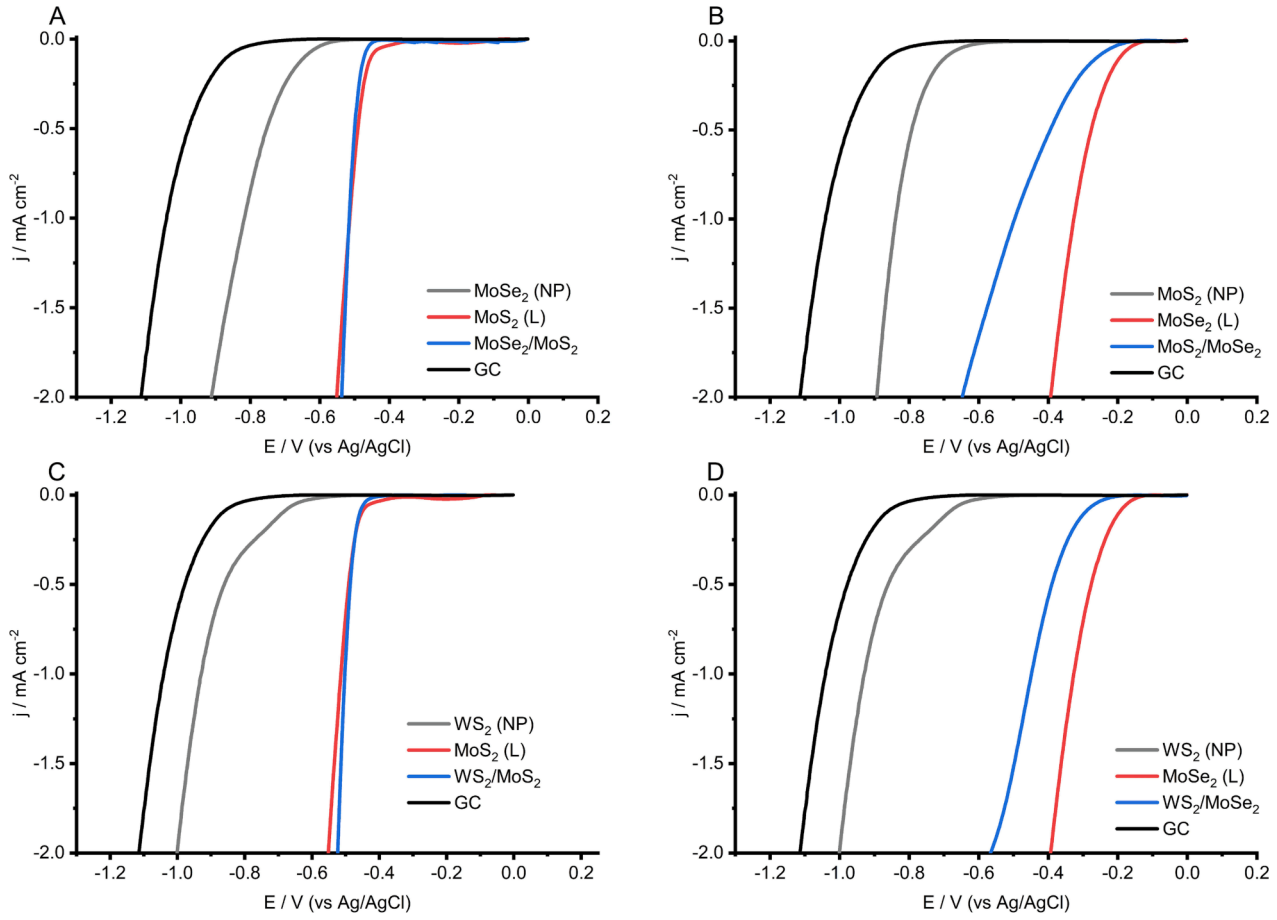

Fig. 3. Linear sweep voltammograms of (A) $MoSe_2/MoS_2$, (B) $MoS_2/MoSe_2$, (C) WS_2/MoS_2 and (D) $WS_2/MoSe_2$ heterolayers as electrocatalysts for the hydrogen evolution reaction in comparison to the TMDs that make them up. This was done in a solution of 10 mM H_2SO_4 and 0.1 M of K_2SO_4 at voltage scan rate of 20 mV s^{-1} for all the scans.

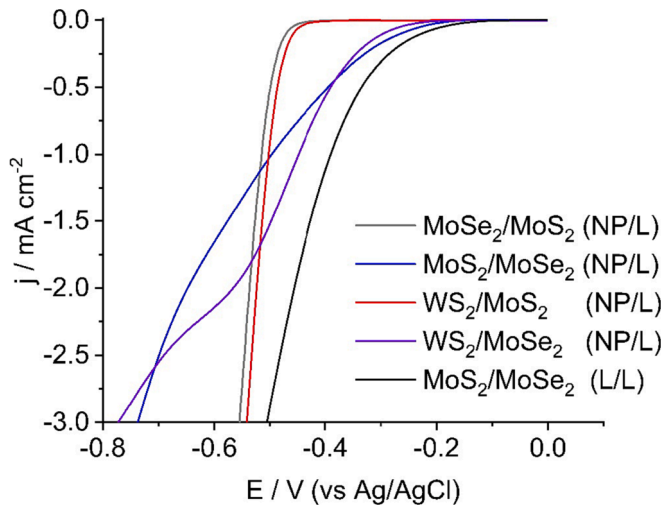

Fig. 4. Overlay of the different heterolayers and how they compare to each other. All conditions were kept the same and the voltammetry was carried out in a 10 mM H_2SO_4 and 0.1 M K_2SO_4 solution and with a Ag/AgCl reference electrode and a graphite rod counter at a scan rate of 20 mV s^{-1}.

Table 1
HER mechanism steps.

Step	Equation	Tafel slope, mV dec^{-1}
Volmer	$H_3O^+ + e^- \rightarrow H_{ads} + H_2O$	120
Heyrovsky	$H_{ads} + H_3O^+ + e^- \rightarrow H_2 + H_2O$	40
Tafel	$H_{ads} + H_{ads} \rightarrow H_2$	30

Table 2
Onset potential and Tafel slope values for the various TMDs and their heterolayers.

Heterolayer	Onset Potential at 0.5 mA cm^{-2} (±0.01)/V	Tafel slope (±0.5)/ mV dec^{-1}	Reported Tafel slopes/mV dec^{-1}	Synthesis method for reported Tafel slopes
$MoSe_2$/ MoS_2 (NP/L)	−0.50	57	289 71	Electrodeposition [33] Hydrothermal and microwave-assisted method [38]
MoS_2/ $MoSe_2$ (NP/L)	−0.39	94	315	Electrodeposition [33]
MoS_2/ $MoSe_2$ (L/L)	−0.34	89	315	Electrodeposition [33]
WS_2/MoS_2 (NP/L)	−0.49	46	72	Chemical bath deposition and RF magnetron sputtering system [46]
$WS_2/MoSe_2$ (NP/L)	−0.39	98	60	Chemical bath and chemical vapor deposition sputtering [31]

step in the HER reaction mechanism as a result of catalysis from the heterolayers. WS_2/MoS_2 and $MoSe_2/MoS_2$ (NP/L) Tafel slope values are closer to the Heyrovsky step value thus indicating that the Heyrovsky is the rate determining step in the HER mechanism. The other heterolayers, that is $MoS_2/MoSe_2$ (L/L), $MoS_2/MoSe_2$ (NP/L) and $WS_2/MoSe_2$ (NP/L) have Tafel slope values which fall between the reported Tafel values for the Volmer and Heyrovsky steps. This suggests a mixture of the Volmer and Heyrovsky steps as rate determining steps in HER reaction mechanism involving these electrocatalysts. All the heterolayers yielded Tafel slopes values less than the previously reported values except for $WS_2/MoSe_2$ heterolayer. Throughout this work, onset potential is defined as the potential (vs Ag/AgCl) at which current density is 0.5 mA cm^{-2}. For most heterolayers, the HER onset value falls between the individual particle dropcast and electrodeposited form apart from the WS_2/MoS_2 (NP/L) heterolayer.

Next, the HER performance of the heterolayered electrodes were investigated via rotating disk voltammetry to determine kinetic performance. A surface modified glassy carbon rotating disk electrode was used to run LSV measurements from 0 to −1.6 V (vs Ag/AgCl) in an acid solution of 10 mM H_2SO_4 and 0.1 M K_2SO_4. Given the nature of the rotating disk electrode, only stable heterolayers such as $MoSe_2/MoS_2$ and WS_2/MoS_2 which could withstand the rotation were used in the study. The rotational speed was varied between 400 and 2000 rpm from 0 to −1.6 V (vs Ag/AgCl) at 20 mV s^{-1} and the resulting voltammograms used for the Koutecky-Levich analysis. Fig. 5 displays the voltammogram resulting from WS_2/MoS_2 heterolayer along with the Koutecky-Levich plot (B) and Tafel graphs (C) used in calculating the rate constant. The standard electrochemical rate constant was calculated to be $k_0 = (3.20 \pm 0.10) \times 10^{-4}$ cm s^{-1} and a transfer coefficient of $\alpha = 0.62 \pm 0.02$. The same was done for $MoSe_2/MoS_2$ heterolayer (Supporting Information, Fig. S9) and a rate constant of $k_0 = (1.73 \pm 0.03) \times 10^{-4}$ cm s^{-1} and a transfer coefficient of $\alpha = 0.85 \pm 0.02$ were calculated. Both WS_2/MoS_2 and $MoSe_2/MoS_2$ heterolayers have resulted in an improved rate constant by an order of magnitude compared to the reported MoS_2 rate constant of $k_0 = (3.17 \pm 0.30) \times 10^{-5}$ cm s^{-1} which had the same preparative method via electrochemical deposition [37]. This highlights the improved catalytic activity of the two heterolayers for the hydrogen evolution reaction.

3.3. SEM and EDS characterization

SEM and EDS characterization were used to gain insight into the atomic components and surface morphology of the heterolayers via imaging and spectrum analysis. SEM images and EDS spectra of the heterolayers are shown on the supporting information (Figs. S14-18). These show the top-view of the heterolayer surfaces: rough surfaces can be observed, and further magnification reveals particles of different sizes thus supporting the non-homogeneity of the heterolayer surfaces. The EDS spectral results confirmed the presence of the different elements arising from the various TMDs used in making the heterolayers. For the $MoSe_2/MoS_2$ heterolayer, molybdenum, sulfur and selenium elements were detected during EDS. Detection of Se in the EDS spectra indicates that there might be dissolution and redeposition of the $MoSe_2$ layer during the electrochemical deposition of the MoS_2 layer. Direct imaging of the WS_2/MoS_2 heterolayer cross-section by FIB-SEM (focused ion beam scanning electron microscope) (**Fig. S19**) showed a single layer of material instead of two distinct layers. This may be due to the dissolution-deposition of the underlayer during the deposition of the overlayer forming a single “alloy-type” layer as reported by Strange [33].

Further characterization was conducted through XPS to determine the elemental compositions of the heterolayers. For the $MoSe_2/MoS_2$ sample, XPS confirmed the presence of Mo, S and Se in the sample as shown in the wide spectra on Fig. 6**(A)**. High resolution spectra of these peaks revealed the Mo 3d, S 2s, S2p, Se 3s and Se 3d peaks. The Mo 3d peak area consisted of the Mo^{4+} at peaks 229 eV and 232 eV along with the Mo^{6+} at 236 eV [11,36,47,48]. The Mo^{6+} is attributed to the presence of MoO_3 in the sample and this is supported by the detection of significant amounts of oxygen in the sample. MoO_3 results from the partial oxidation of the layers when in contact with oxygen. S 2s and Se 3s were also detected in this spectrum at 228 eV and 232 respectively [47,49]. Two other chemical states of Se were detected, i.e., the Se 3d and Se 3p. For Se 3d, the peak of the spin–orbit doublet of Se $3d_{3/2}$ and Se $3d_{5/2}$ was detected with their peaks at 55.3 and 54.1 eV respectively [38,50]. To derive the elemental composition of the sample, accurate

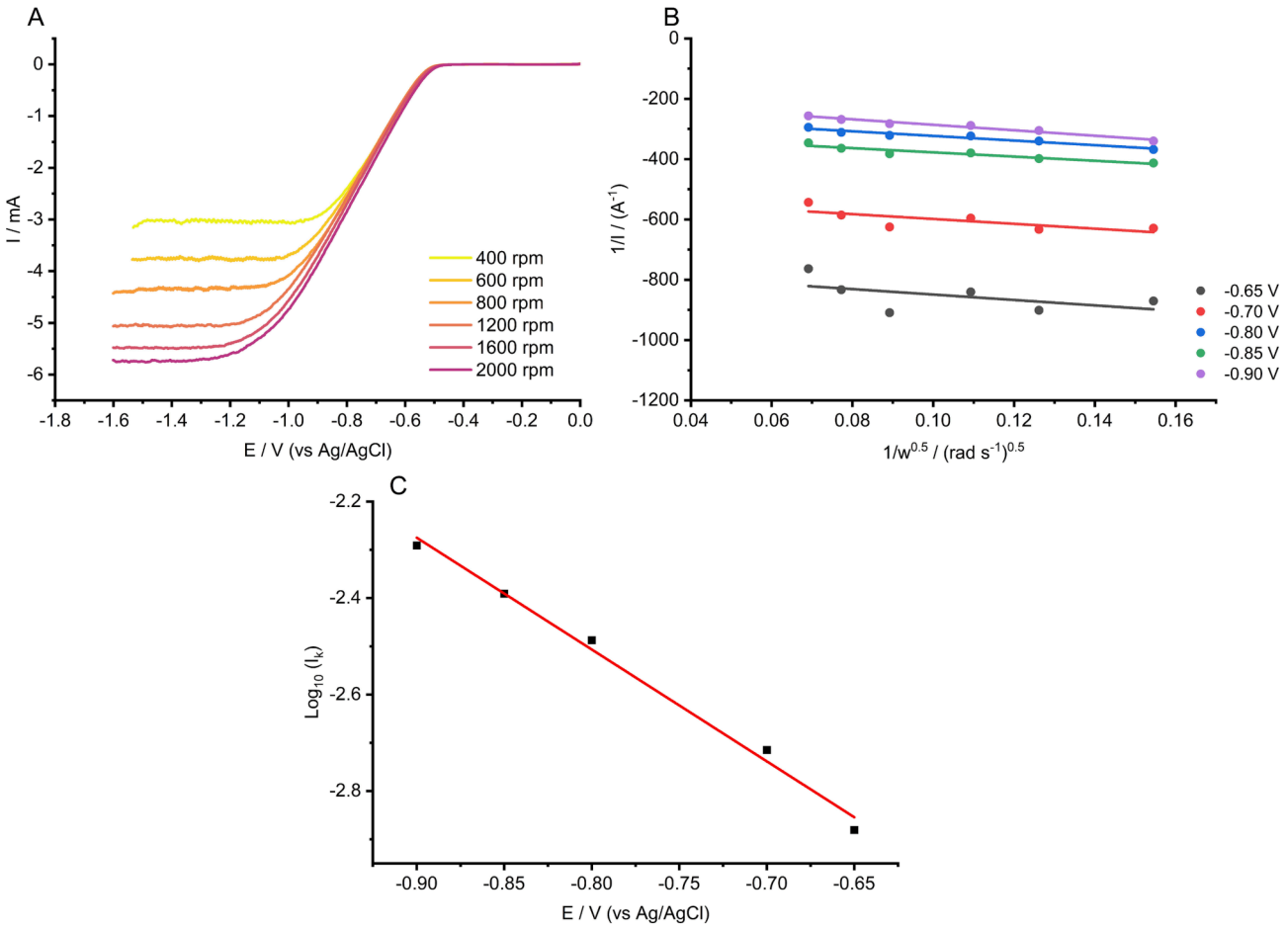

Fig. 5. (A). HER voltammograms at various rotation rates using the WS_2/MoS_2 heterolayer electrocatalyst in a solution of 10 mM H_2SO_4 and 0.1 M K_2SO_4. **(B).** Koutecky-Levich plot resulting from the voltammograms in (A). **(C).** Tafel plot from using the intercepts and potentials data in (B). A best fit line was drawn with the resulting equation $Log(I_k) = -2.32E - 4.36$, from which the electrochemical rate constant was calculated.

quantification would normally involve the analysis of the S 2p and Se 3p peaks. However, here these peaks overlap which makes peak deconvolution difficult: hence the S 2s and Se 3d peaks have been used for quantification [33]. This is also the case for the $MoSe_2/MoS_2$ sample. The S 2s: Se 3p peak area ratio for the $MoS_2/MoSe_2$ was calculated to be 1.0:1.9, while for the $MoSe_2/MoS_2$ it was 7.9:1.0. The difference is due to the amount of TMD film electrodeposited which is significantly more in comparison to the dropcast nanoparticles.

alysis of the wide survey spectrum of the WS_2/MoS_2 heterolayer sample confirmed the presence of Mo, W and S elements which were detected via SEM-EDS. High resolution spectra of the Mo peak area also showed both Mo^{4+} and Mo^{6+} species along with the S 2s peak as displayed on **Fig. S12**. For this sample, partial oxidation also occurred hence the Mo^{6+} peaks observed. The chemical composition could not be determined since the S^{2-} was a common anion to both layers but the relative amounts of W^{4+} and Mo^{4+} could be used to determine the ratio of WS_2 to MoS_2 in the heterolayer sample. The ratio of W^{4+} to Mo^{4+} was calculated to be 1:2.7 thereby showing there is approximately 3 times more MoS_2 in the WS_2/MoS_2 heterolayer sample.

Spectroscopic ellipsometry was used to determine the thickness of the electrodeposited films (see Fig. 7). For the $MoS_2/MoSe_2$ (L/L) heterolayer, a total layer thickness of (43.3 ± 4.4) nm with the MoS_2 film having a thickness of (25.5 ± 5.4) nm and (17.8 ± 3.4) nm for $MoSe_2$. The root mean squared error (MSE) value of 2.38 indicates a good fit of the model to the experimental data.

4. Conclusion

Transition metal dichalcogenide heterostructures were investigated for their HER catalytic activity as well as determining the reaction kinetics resulting from them. Two methods of forming the heterolayers were used: one consisting of a dropcast nanoparticle layer with an electrodeposited layer of a different TMD on top ('NP/L'), and the second was obtained by sequential electrodeposition of layers of the two different TMDs ('L/L'). The stability of the resulting heterolayers was tested in an acidic solution and it was observed that those with a film of $MoSe_2$ had low stability while those with a film of MoS_2 were very stable even after 10 consecutive CV scans. Heterolayers with a film of MoS_2 displayed an improved HER ability when compared to the starting TMD materials. An earlier onset potential for HER was also observed for them. The resulting reaction kinetics due to the heterolayers was investigated and these included Tafel analysis and electrochemical rate constant calculation. WS_2/MoS_2 and $MoSe_2/MoS_2$ heterolayers registered rate constants of $(3.20 \pm 0.10) \times 10^{-4}$ cm s^{-1} and $(1.73 \pm 0.03) \times 10^{-4}$ cm s^{-1} respectively, which was an improvement of an order of magnitude compared to the reported rate constant of electrodeposited MoS_2. This further showed the improved HER catalytic activity of the heterolayers and how there is still room for improvement when it comes to TMDs.

CRediT authorship contribution statement

Tshiamo Manyepedza: Writing – original draft, Validation, Investigation, Formal analysis, Data curation, Conceptualization. **Thomas**

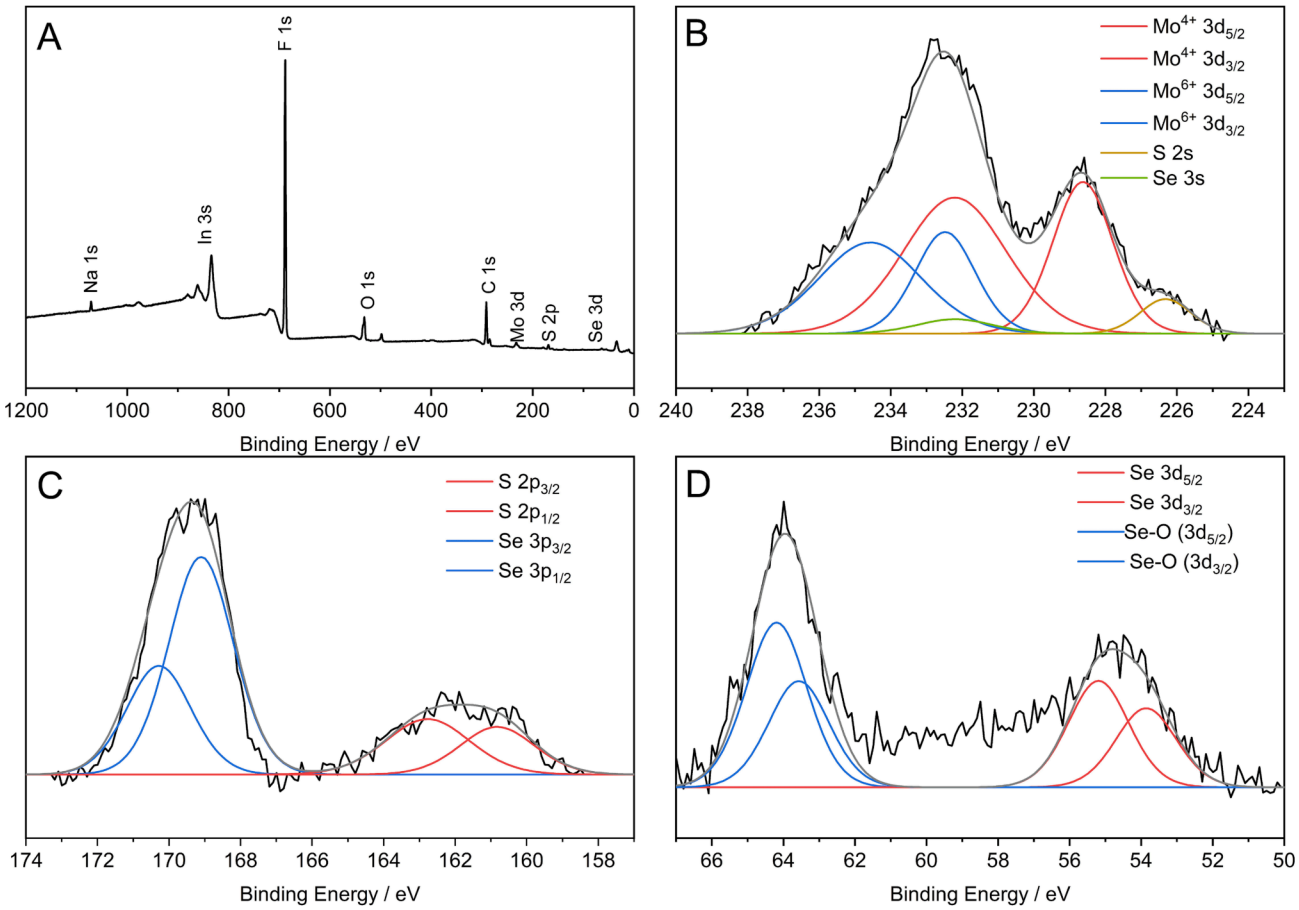

Fig. 6. **(A)** Wide area spectra of the $MoSe_2/MoS_2$ sample displaying all the elements in it. High resolution spectra of the **(B)** Mo 3d peak, **(C)** S 2p peak and the **(D)** Se 3d peaks from the sample $MoSe_2/MoS_2$.

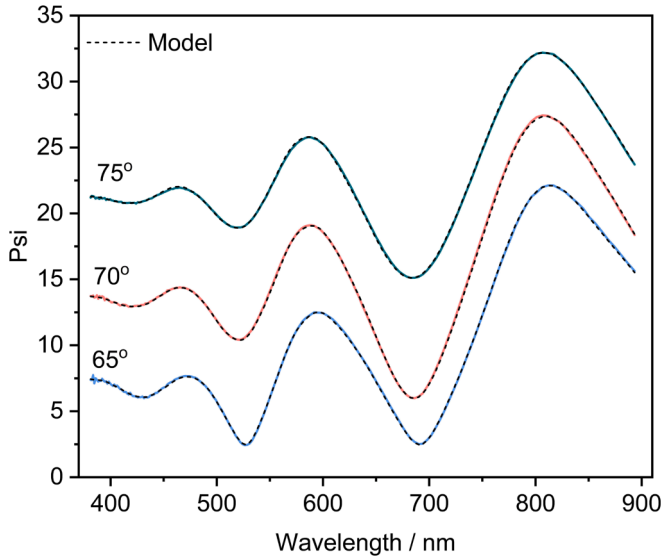

Fig. 7. Model fitting result of the simulated data (———) against experimental data. The experimental data was collected at three different angles and then fitted using Tauc-Lorentz model to determine the sample thickness.

Auvray: Writing – review & editing, Resources, Investigation. **Tomislav Friščić:** Writing – review & editing, Supervision. **Neil V. Rees:** Writing – review & editing, Visualization, Conceptualization.

Declaration of competing interest

The authors declare that they have no known competing financial interests or personal relationships that could have appeared to influence the work reported in this paper.

Data availability

The authors do not have permission to share data.

Acknowledgements

The authors wish to thank Dr Nigel Neate (Nanoscale and Microscale Research Centre, University of Nottingham) and Dr Marcos Fernandez-Villamarin (School of Chemical Engineering, University of Birmingham) for assistance in performing FIB-SEM and Spectroscopic Ellipsometry measurements respectively. NVR thanks The Leverhulme Trust (RPG-2019-146) and TM thanks the Government of Botswana (TR184730) for funding. TA and TF acknowledge support of the Leverhulme Trust (Leverhulme International Professorship, LIP-2021-011) and the University of Birmingham.

Appendix A. Supplementary data

Supplementary data to this article can be found online at https://doi.org/10.1016/j.elecom.2024.107678.

References

[1] X. Lin, F. Wang, X. Shan, Y. Miao, X. Chen, M. Yan, L. Zhang, K. Liu, J. Luo, K. Zhang, High-performance photodetector and its optoelectronic mechanism of MoS_2/WS_2 vertical heterostructure, Appl. Surf. Sci. 546 (2021) 149074.

[2] Q. Lv, X. Wu, J. Tan, B. Liu, L. Gan, J. Li, Z.H. Huang, F. Kang, L. Ruitao, Ultrasensitive molecular sensing of few-layer niobium diselenide, J. Mater. Chem. A 9 (2021) 2725–2733.

[3] C. Bradac, Z.Q. Xu, I. Aharonovich, Quantum energy and charge transfer at two-dimensional interfaces, Nano Lett. 21 (2021) 1193–1204.

[4] Q. Fu, J. Han, X. Wang, P. Xu, T. Yao, J. Zhong, W. Zhong, S. Liu, T. Gao, Z. Zhang, L. Xu, B. Song, 2D Transition metal dichalcogenides: design, modulation, and challenges in electrocatalysis, Adv. Mater. 33 (2021) 1907818.

[5] Y. Shi, H. Li, L.J. Li, Recent advances in controlled synthesis of two-dimensional transition metal dichalcogenides via vapour deposition techniques, Chem. Soc. Rev. 44 (2015) 2744–2756.

[6] Q. Liang, Q. Zhang, X. Zhao, M. Liu, A.T. Wee, Defect engineering of two-dimensional transition-metal dichalcogenides: applications, challenges, and opportunities, ACS Nano 15 (2021) 2165–2181.

[7] A.V. Kolobov, J. Tominaga, Two-Dimensional Transition-Metal Dichalcogenides, Springer International Publishing, 2016.

[8] M. Chhlowalla, H.S. Shin, G. Eda, L.J. Li, K.P. Loh, H. Zhang, The chemistry of two-dimensional layered transition metal dichalcogenide nanosheets, Nat. Chem. 5 (2013) 263–275.

[9] T.H.M. Lau, X. Lu, J. Kulhavý, S. Wu, L. Lu, T.S. Wu, R. Kato, J.S. Foord, Y.L. Soo, K. Suenaga, S.C.E. Tsang, Transition metal atom doping of the basal plane of MoS_2 monolayer nanosheets for electrochemical hydrogen evolution, Chem. Sci. 9 (2018) 4769–4776.

[10] D. Merki, S. Fierro, H. Vrubel, X. Hu, Amorphous molybdenum sulfide films as catalysts for electrochemical hydrogen production in water, Chem. Sci. 2 (2011) 1262–1267.

[11] D. Escalera-López, Z. Lou, N.V. Rees, Benchmarking the activity, stability, and inherent electrochemistry of amorphous molybdenum sulfide for hydrogen production, Adv. Energy. Mater. 9 (2019) 1802614.

[12] B. Hinnemann, P.G. Moses, J. Bonde, K.P. Jorgensen, J.H. Nielsen, S. Horch, I. Chorkendorff, J.K. Norskov, Biomimetic hydrogen evolution: MoS2 nanoparticles as catalyst for hydrogen evolution, J. Am. Chem. Soc. 127 (2005) 5308–5309.

[13] D. Voiry, M. Salehi, R. Silva, T. Fujita, M. Chen, T. Asefa, V.B. Shenoy, G. Eda, M. Chhowalla, Conducting MoS_2 nanosheets as catalysts for hydrogen evolution reaction, Nano Lett. 13 (2013) 6222–6227.

[14] T. Li, G. Galli, Electronic properties of MoS2 nanoparticles, J. Phys. Chem. C 111 (2007) 16192–16196.

[15] M.B. Wazir, M. Daud, S. Safeer, F. Almarzooqi, A. Qurashi, Review on 2D molybdenum diselenide (MoSe2) and its hybrids for green hydrogen (H2) generation applications, ACS Omega 7 (2022) 16856–16865.

[16] X. Xia, L. Wang, N. Sui, V.L. Colvin, W. Yu, Recent progress in transition metal selenide electrocatalysts for water splitting, Nanoscale 12 (2020) 12249–12262.

[17] A. Eftekhari, Molybdenum diselenide (MoSe2) for energy storage, catalysis, and optoelectronics, Appl. Mater. Today. 8 (2017) 1–17.

[18] D. Xiao, C. Huang, Y. Luo, K. Tang, Q. Ruan, G. Wang, P.K. Chu, Atomic-scale intercalation of graphene layers into $MoSe_2$ nanoflower sheets as a highly efficient catalyst for hydrogen evolution reaction, ACS Appl. Mater. Interfaces 12 (2019) 2460–2468.

[19] M.T. Shu, M. Pumera, Bottom-up electrosynthesis of highly active tungsten sulfide films for hydrogen evolution, ACS Appl. Mater. Interfaces 8 (2016) 3948–3957.

[20] M. Velicky, R.A. Dryfe, Electrochemistry of 2D nanomaterials, Front. Nanosci. 18 (2021) 485–536.

[21] G. Li, D. Zhang, Q. Qiao, Y. Yu, D. Peterson, A. Zafar, R. Kumar, S. Curtarolo, F. Hunte, S. Shannon, Y. Zhu, W. Yang, L. Cao, All the catalytic active sites of MoS_2 for hydrogen evolution, J. Am. Chem. Soc. 138 (2016) 16632–16638.

[22] A. Ambrosi, Z. Sofer, M. Pumera, 2H → 1T phase transition and hydrogen evolution activity of MoS_2, $MoSe_2$, WS_2 and WSe_2 strongly depends on the MX_2 composition, Chem. Commun. 51 (2015) 8450–8453.

[23] Q. Jin, N. Liu, B. Chen, D. Mei, Mechanisms of semiconducting 2H to metallic 1T phase transition in two-dimensional MoS_2 nanosheets, J. Phys. Chem. c. 122 (2018) 28215–28224.

[24] M.A. Py, R.R. Hearing, Structural destabilization induced by lithium intercalation in MoS_2 and related compounds, Can. J. Phys. 61 (1983) 76–84.

[25] C. Tan, Z. Luo, A. Chaturvedi, Y. Cai, Y. Du, Y. Gong, Y. Huang, Z. Lai, X. Zhang, L. Zheng, X. Qi, M.H. Goh, S. Han, C. Kloc, H. Zhang, Preparation of high-percentage 1T-phase transition metal dichalcogenide nanodots for electrochemical hydrogen evolution, Adv. Mater. 30 (2018) 1705509.

[26] Z. Qian, L. Jiao, L. Xie, Phase engineering of two-dimensional transition metal dichalcogenides, Chin. J. Chem. 38 (2020) 753–760.

[27] H. Terrones, F. Lopez-Urias, M. Terrones, Novel hetero-layered materials with tunable direct band gaps by sandwiching different metal disulfides and diselenides, Sci. Rep. 3 (2013) 1549.

[28] B. Amin, N. Singh, U. Schwingenschlogl, Heterostructures of transition metal dichalcogenides, Phys. Rev. B 92 (2015) 075439.

[29] H.P. Komsa, A.V. Krasheninnikov, Electronic structures and optical properties of realistic transition metal dichalcogenide heterostructures from first principle, Phys. Rev. B. 88 (2015) 085318.

[30] J. He, K. Hummer, C. Franchini, Stacking effects on the electronic and optical properties of bilayer transition metal dichalcogenides MoS_2, $MoSe_2$, WS_2 and WSe_2, Phys. Rev. B. 89 (2014) 075409.

[31] D. Vikraman, S. Hussain, S.A. Patil, L. Truong, A.A. Arbab, S.H. Jeong, S.H. Chun, J. Jung, H.S. Kim, Engineering $MoSe_2/WS_2$ hybrids to replace the scarce platinum electrode for hydrogen evolution reactions and dye-sensitized solar cells, ACS Appl. Mater. Interfaces. 13 (2021) 5061–5072.

[32] G. Zhao, P. Li, K. Rui, Y. Chen, S.X. Dou, W. Sun, $CoSe_2/MoSe_2$ heterostructures with enriched water adsorption/dissociation sites towards enhanced alkaline hydrogen evolution reaction, Chem. Eur. J. 24 (2018) 11158–11165.

[33] L.E. Strange, S. Garg, P. Kung, M. Ashaduzzaman, G. Szulczewski, S. Pan, Electrodeposited transition metal dichalcogenides for use in hydrogen evolution electrocatalysts, J. Electrochem. Soc. 169 (2022) 026510.

[34] D. Belanger, G. Laperriere, B. Marsan, The electrodeposition of amorphous molybdenum sulfide, J. Electroanal. Chem. 347 (1993) 165–183.

[35] C. Li, M. Iqbal, J. Lin, X. Luo, B. Jiang, V. Malgras, K.C.W. Wu, J. Kim, Y. Yamauchi, Electrochemical deposition: an advanced approach for templated synthesis of nanoporous metal architectures, Acc. Chem. Res. 51 (2018) 1764–1773.

[36] X. Hu, H. Vrubel, Growth and activation of an amorphous molybdenum sulfide hydrogen evolving catalyst, ACS Catal. 3 (2013) 2002–2011.

[37] T. Manyepedza, J.M. Courtney, A. Snowdon, C.R. Jones, N.V. Rees, Impact electrochemistry of MoS_2: electrocatalysis and hydrogen generation at low overpotentials, J. Phys. Chem. C 126 (2022) 17942–17951.

[38] M.D. Sharma, C. Mahala, M. Basu, 2D Thin sheet heterostructures of MoS_2 on $MoSe_2$ as efficient electrocatalyst for hydrogen evolution reaction in wide pH range, Inorg. Chem. 59 (2020) 4377–4388.

[39] M.R. Gao, J.X. Liang, Y.R. Zheng, Y.F. Xu, Q. Gao, J. Li, S.H. Yu, An efficient molybdenum disulfide/cobalt diselenide hybrid catalyst for electrochemical hydrogen generation, Nat. Commun. 6 (2015) 5982.

[40] J. Yang, C. Wang, H. Ju, Y. Sun, S. Xing, J. Zhu, Q. Yang, Integrated quasiplane heteronanostructures of $MoSe_2/Bi_2Se_3$ hexagonal nanosheets: synergetic electrocatalytic water splitting and enhanced supercapacitor performance, Adv. Funct. Mater. 27 (2017) 1703864.

[41] S. Li, W. Zang, X. Liu, S.J. Pennycook, Z. Kou, C. Yang, C. Guan, J. Wang, Heterojunction engineering of $MoSe_2/MoS_2$ with electronic modulation towards synergetic hydrogen evolution reaction and supercapacitance performance, Chem. Eng. J. 359 (2019) 1419–1426.

[42] L. Zhang, J. Zhu, Z. Wang, W. Zhang, 2D $MoSe_2$/CoP intercalated nanosheets for efficient electrocatalytic hydrogen production, Int. J. Hydrogen Energy. 45 (2020) 19246–19256.

[43] Y. Li, H. Wang, L. Xie, Y. Liang, G. Hong, H. Dai, MoS_2 nanoparticles grown on graphene: an advanced catalyst for the hydrogen evolution reaction, J. Am. Chem. Soc. 133 (2011) 7296–7299.

[44] B.E. Conway, B.V. Tilak, Interfacial processes involving electrocatalytic evolution and oxidation of H-2 and the role of chemisorbed H, Electrochim. Acta. 47 (2002) 3571–3594.

[45] N. Dubouis, A. Grimaud, The hydrogen evolution reaction: from material to interfacial descriptors, Chem. Sci. 10 (2019) 9165–9181.

[46] D. Vikraman, S. Hussain, K. Akbar, L. Truong, A. Kathalingam, S.H. Chun, J. Jung, H.J. Park, H.S. Kim, Improved hydrogen evolution reaction performance using MoS_2–WS_2 heterostructures by physicochemical process, ACS Sustain. Chem. Eng. 6 (2018) 8400–8409.

[47] A. Ambrosi, M. Pumera, Templated electrochemical fabrication of hollow molybdenum sulfide microstructures and nanostructures with catalytic properties for hydrogen production, ACS Catal. 6 (2016) 3985–3993.

[48] J.F. Moulder, W.F. Stickle, P.E. Sobol, K.D. Bomben, Handbook of X-ray Photoelectron Spectroscopy, Perkin-Elmer Corporation, Minnesota, 1992.

[49] T. Weber, J.C. Muijsers, J.W. Niemantsverdriet, Structure of amorphous MoS_3, J. Phys. Chem. 99 (1995) 9194–9200.

[50] J. Rodriguez-Pereira, R. Zazpe, J. Charvot, F. Bures, J.M. Macak, Molybdenum diselenide thin films grown by atomic layer deposition: an XPS analysis, Surf. Sci. Spectra. 27 (2020) 024006.